Atmos. Chem. Phys., 24, 13183–13198, 2024
https://doi.org/10.5194/acp-24-13183-2024

Atmospheric Chemistry and Physics
Open Access
EGU

Exploring HONO production from particulate nitrate photolysis in representative regions of China: characteristics, influencing factors, and environmental implications

Bowen Li, Jian Gao, Chun Chen, Liang Wen, Yuechong Zhang, Junling Li, Yuzhe Zhang, Xiaohui Du, Kai Zhang, and Jiaqi Wang

State Key Laboratory of Environmental Criteria and Risk Assessment, Chinese Research Academy of Environmental Sciences, Beijing 100012, China

Correspondence: Kai Zhang (zhangkai@craes.org.cn) and Jiaqi Wang (wang.jiaqi@craes.org.cn)

Received: 10 July 2024 – Discussion started: 12 August 2024
Revised: 11 October 2024 – Accepted: 14 October 2024 – Published: 29 November 2024

Abstract. The production mechanism of atmospheric nitrous acid (HONO), an important precursor of the hydroxyl radical (OH), remains controversial. Few studies have explored the effects of particulate nitrate photolysis on HONO sources under different environment conditions across China. In this work, the photolysis rate constant of particulate nitrate for HONO production ($J_{NO_3^--HONO}$) was determined through a photochemical reaction system with $PM_{2.5}$ samples collected from five representative sites in China. We developed a method to correct and quantify the "shadowing effect" – potential light extinction within aerosol layers under heavy $PM_{2.5}$ loading conditions on the filters – for $J_{NO_3^--HONO}$ measurements, showing that elemental carbon (EC), the dominant light-absorbing component in $PM_{2.5}$, plays a dominant role in it. The corrected $J_{NO_3^--HONO}$ values varied with the sampling period and location over a wide range, from 1.6×10^{-6} to 1.96×10^{-4} s^{-1}, with a mean (±1 SD) of $1.71\ (\pm 2.36) \times 10^{-5}$ s^{-1}. Chemical compositions, specifically those concerning nitrate loading and organic components, affected the production of HONO through particulate nitrate photolysis: high $J_{NO_3^--HONO}$ values were generally associated with $PM_{2.5}$ samples with a high organic carbon (OC) / NO_3^- ratio ($R^2 = 0.86$). We suggest that the parameterization equation between $J_{NO_3^--HONO}$ and the OC / NO_3^- ratio established in this work can be used to estimate $J_{NO_3^--HONO}$ under different aerosol chemical conditions, thus reducing the uncertainty in exploring daytime HONO sources. This study confirms that the photolysis of particulate nitrate can be a potential daytime HONO source in rural or southern urban sites, which are characterized by $PM_{2.5}$ containing high proportions of organic matter.

1 Introduction

Gaseous nitrous acid (HONO) is an important nitrogen-containing trace gas in the troposphere and can produce the hydroxyl radical (OH) through photolysis, thus stimulating the enhancement of atmospheric oxidation and the formation of secondary aerosols (Fu et al., 2019; Slater et al., 2020; Ren et al., 2003; Li et al., 2011; Su et al., 2011). In recent years, the contribution of HONO to atmospheric oxidation under heavily polluted conditions has attracted great attention (Villena et al., 2011; Fu et al., 2019; Slater et al., 2020). Even though observational research on HONO has been conducted for nearly 40 years, the understanding of HONO's daytime sources remains controversial (Fu et al., 2019; Wang et al., 2017; Mora Garcia et al., 2021). Numerous mechanisms have been proposed to explain the extremely high HONO concentrations at noon, including direct combustion emissions (Kurtenbach et al., 2001; Liang et al., 2017; Liao

et al., 2021), gas-phase reactions of NO and OH radicals (Li et al., 2011; Zhang et al., 2016), heterogeneous reactions of NO_2 (Wang et al., 2017; Ammann et al., 1998; Monge et al., 2010; Stemmler et al., 2006), soil emissions (Su et al., 2011; Oswald et al., 2013; Donaldson et al., 2014; Kim and Or, 2019), and the photolysis of HNO_3 and nitrate on aerosol or ground surfaces (Zhou et al., 2003, 2011; Ye et al., 2016b, a, 2017).

Particulate nitrate, which has conventionally been considered the ultimate oxidation product of NO_x, can rapidly photolyze and recycle NO_x or HONO back to the gas phase (Andersen et al., 2023; Handley et al., 2007; Beine et al., 2006; Ye et al., 2016a, b, 2017; Gu et al., 2022b) at a rate 10 to 300 times faster than the photolysis rate of gaseous HNO_3 ($\sim 7 \times 10^{-7}\,s^{-1}$) under typical tropical noontime conditions (Finlayson-Pitts and Pitts, 2000). Recently, some field, laboratory, and modeling works have proposed that the photolysis of particulate nitrate can be an important in situ source of HONO in rural, suburban, and urban environments (Ye et al., 2016b; Mora Garcia et al., 2021; Liu et al., 2019; Bao et al., 2018; Wang et al., 2017). Fu et al. (2019) found that the photolysis of HNO_3 and nitrate in the atmosphere and that deposited on surfaces was the dominant HONO source at noon and during the afternoon, contributing to more than 50 % of the simulated HONO. However, there are large discrepancies in estimating the rate constants in the atmosphere (Gen et al., 2022). In New York, Ye et al. (2017) reported that the photolysis rates of particulate nitrate in clean areas were 2 orders of magnitude higher than those in polluted areas, ranging from 6.2×10^{-6} to $5.0 \times 10^{-4}\,s^{-1}$, with a median of $8.3 \times 10^{-5}\,s^{-1}$. The proposed rate constants for nitrate photolysis based on aircraft observations over South Korea ranged from 7×10^{-6} to $2.1 \times 10^{-5}\,s^{-1}$ (Romer et al., 2018). Shi et al. (2021) derived a rate constant ($< 2 \times 10^{-5}\,s^{-1}$) based on chamber experiments but found a limited role for this mechanism in HONO production. The uncertainty in the HONO production rate from the photolysis of particulate nitrate can reach up to $1.4\,ppbv\,h^{-1}$ and greatly affect the accuracy of HONO source analysis (Liu et al., 2019; Lee et al., 2016; Ye et al., 2016a). The highly variable photolysis rate constant of particulate nitrate is closely associated with environmental conditions and the aerosol's chemical or physical characteristics, such as relative humidity (RH), aerosol acidity, light intensity, and coexisting components (organic components, halogens, etc.) (Gelencsér et al., 2003; Ye et al., 2016a; Bao et al., 2020; Wang et al., 2021; Reeser et al., 2013). Elucidating the mechanism and dominant factors controlling the photolysis of particulate nitrate is important to accurately estimate HONO production rates from nitrate photolysis, thus improving estimations of HONO budgets.

In general, the photolysis rate constant of particulate nitrate is derived though photochemical experiments using bulk particle samples collected on filters (Ye et al., 2017; Bao et al., 2018). Compared with suspended particles in the ambient atmosphere, $PM_{2.5}$ particles collected on aerosol filters may present a multiple-layer structure, especially in heavy air pollution conditions (Bao et al., 2018). The light-absorbing species within $PM_{2.5}$ particles can hinder the light absorption of particulate nitrate in the lower layers of the filter sample, thus inhibiting the photolysis of particulate nitrate, a phenomenon called the "shadowing effect" (Ye et al., 2017). The shadowing effect of aerosol filters collected in clean air conditions may be negligible, but this effect should be evaluated and quantified in heavy haze conditions, where the aerosol loading is much higher for the same sampling time. However, previous works have generally ignored this shadowing effect.

According to previous field observations, the $PM_{2.5}$ chemical composition, especially that concerning particulate nitrate (NO_3^-), has shown obvious spatial differences across China (Wang et al., 2022a, b; Y. Wang et al., 2022; Wang et al., 2016; Cheng et al., 2024). As one of the key industrial development areas in China, the Pearl River Delta (PRD) region has a great number of large-scale industrial parks dominated by the chemical industry, resulting in significant emissions of volatile organic compounds (VOCs) and a high proportion of organic matter (OM) in $PM_{2.5}$. In the North China Plain (NCP), particulate nitrate (NO_3^-) has surpassed sulfate (SO_4^{2-}) and OM to become the dominant $PM_{2.5}$ component in recent years (Wang et al., 2022b). Until now, the investigation of particulate nitrate photolysis in different atmospheric environments has been limited in China, and the influence of chemical or physical characteristics of aerosols on HONO production has been unclear. In this work, to shed light on the contribution of particulate nitrate photolysis to daytime HONO sources, we examined the photolysis rate constant for HONO based on photochemical experiments using $PM_{2.5}$ samples collected from five typical sites in China. In addition, the shadowing effect due to increasing aerosol particle loading on the filters was quantified. After correcting for this effect, the influence of various environmental conditions, including those concerning particulate nitrate, organic matter, and aerosol acidity, on the formation of HONO was investigated, and the possible role of this photolytic process as a source of HONO was also examined.

2 Method

2.1 Sampling and filter treatment

The ambient $PM_{2.5}$ was collected on Teflon or quartz filters during fall–winter seasons at five representative sites, i.e., Beijing, Wangdu, Xinxiang, Guangzhou, and Changji, which are shown in Fig. 1a and described in detail in the Supplement. These cities are located in the North China Plain (NCP), with Beijing as an urban site and Wangdu as a rural one; central China; the Pearl River Delta (PRD) region; and northwestern China, respectively. The sampling flow rates ranged from 16.7 to $1050\,L\,min^{-1}$, the sampling times from 9 to 23 h, and the overall sampling volumes of air from 8 to

1450 m^3 to collect a very wide range of particulate nitrate loadings. The comparison experiments between Teflon and quartz filters were conducted, and no significant differences in HONO production rates from particulate nitrate photolysis were found ($T < 0.01$). The sampling settings employed in Wangdu were designed to quantify the shadowing effect (Fig. 1b). In Wangdu, $PM_{2.5}$ was collected at a flow rate of 16.7 L min^{-1} with four channels (A, B, C, and D). Channels A and B were set for daytime (08:00–17:00 LT) and nighttime (18:00–07:00 LT) $PM_{2.5}$ samples, respectively, and the other two channels were for "all-day" $PM_{2.5}$ samples (including the timings 08:00–17:00 and 18:00–07:00 LT). A total of 158 effective $PM_{2.5}$ samples were obtained in this study. These aerosol filter samples were labeled and stored at −20 °C in the freezer.

Fractions with a given surface area from each filter sample were used to perform photochemical reaction experiments and an analysis of aerosol chemical components. For each $PM_{2.5}$ sample, fractions with a given surface area were rinsed with deionized water and then sonicated for 15 min. The quantity of water-soluble ions, including Na^+, NH_4^+, K^+, Mg^{2+}, Ca^{2+}, Cl^-, NO_3^-, and SO_4^{2-}, were measured using ion chromatography (IC; Thermo Scientific Dionex ICS-2100). To measure the values of carbon components, including those of organic carbon (OC) and elemental carbon (EC), part (0.5024 cm^2) of each filter was detected using a thermal–optical carbon analyzer (DRI (Desert Research Institute) Model 2015). The concentration of OM was obtained by multiplying the OC concentration by a factor of 1.6 (Li et al., 2021). The $PM_{2.5}$ concentration was estimated using the sum of all the water-soluble ions and carbon components. The surface concentration of $PM_{2.5}$ and its components on aerosol filters was calculated by dividing the absorbed loading by the geometric area of the aerosol filter sample (μg cm^{-2}).

2.2 Photochemical reaction system

A custom-made cylindrical quartz vessel was used as the photochemical flow reactor (Fig. 1c). The diameter of the reactor was 10 cm, and the depth was 2.5 cm, with a cell volume of ∼200 mL. A xenon lamp (300 W) was placed 20 cm above the reactor as the light source. The light was filtered with a Pyrex sleeve to remove heat-generating infrared light. The effective light intensity in the center of the flow reactor, where aerosol samples were placed, was measured (by a calibrated optical power meter) to be about 0.5 times higher (1.5 kW m^{-2}) than that at noon under tropical conditions on the ground (with a solar elevation angle of 0°). Synthetic air, composed of ultrahigh-purity nitrogen and ultrahigh-purity oxygen mixed at a ratio of 79 : 21, was used as the carrier gas. The relative humidity (RH) in the airflow was adjusted using a water bubbler and monitored with an online RH sensor (HMT130, Vaisala). The aerosol filter sample was exposed to the solar simulator radiation for 20 min. The photochemical reaction experiment for each sample was repeated 2–3 times with different fractions from the same sample. The gaseous product (i.e., HONO) released during the experiment was flushed out of the reactor by the carrier gas and was detected online by a custom-built HONO analyzer, which had been used in several measurements previously (W. Zhang et al., 2020; Li et al., 2021).

2.3 HONO production from the photolysis of particulate nitrate

The production rates (nmol h^{-1}) of HONO from particulate nitrate photolysis (P_{HONO}) were calculated from their time-integrated signals above the baseline over the period of light exposure:

$$P_{HONO} = \frac{F_g \times 60}{V_m(t_2 - t_1)} \int_{t_1}^{t_2} C_{HONO} dt, \quad (1)$$

where F_g (L min^{-1}) is the flow rate of the carrier gas; V_m (24.5 L mol^{-1}) is the molar volume of gas at 25 °C and under 1 atm of pressure; t_1 and t_2 (minutes) are the starting and ending times of the irradiation, respectively; and C_{HONO} (parts per billion) is the online-measured concentration of HONO. With a flow rate of 2.5 L min^{-1}, the residence time in the reaction system was around ∼5 s. The photolytic loss of HONO was less than 5 %; thus, no correction was made in the calculation of HONO production.

The photolysis rate constant of particulate nitrate leading to HONO production ($J_{NO_3^--HONO}$; s^{-1}) was calculated using the following equation:

$$J_{NO_3^--HONO} = \frac{P_{HONO}}{N_{NO_3^-} \times 3600}, \quad (2)$$

where $N_{NO_3^-}$ (moles) is the amount of NO_3^- in the tested $PM_{2.5}$ sample. In principle, the photolysis rate constant should be calculated based on the amount of NO_3^- that is reachable by the irradiation. However, the amount of light-reachable NO_3^- in the $PM_{2.5}$ sample was hard to quantify. In this work, the deviation of $J_{NO_3^--HONO}$ due to the overestimation of the amount of NO_3^- under light irradiation, referred to as the shadowing effect, will be corrected in Sect. 3.1.

3 Results

3.1 Quantifying the influence of the shadowing effect

HONO production occurring within the first 20 min of irradiation during the photochemical experiment was investigated using $PM_{2.5}$ samples collected from five typical sites in China. Figure 2a shows a typical profile of the changes in HONO concentration in the reaction system. When the

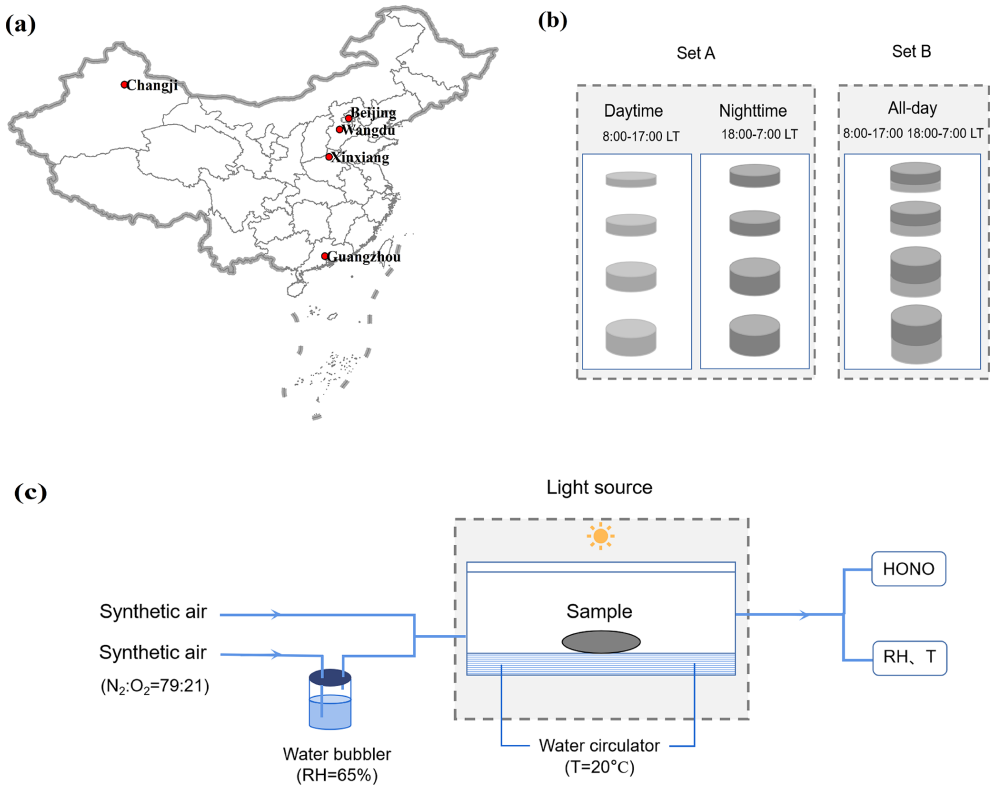

Figure 1. **(a)** Location map of the five representative sampling sites in China. **(b)** The sampling settings used to quantify the shadowing effect in Wangdu. **(c)** A schematic diagram of the photochemical experimental setup.

light was turned on, HONO concentration in the reactor increased immediately, before leveling off and slightly decaying afterwards. After the light was turned off, HONO generation stopped immediately, and the signal nearly returned to its baseline level. Previous works have revealed that the decay of HONO generation during light exposure periods does not result from the evaporation loss of particulate nitrate (Ye et al., 2017) but is mainly related to the inhomogeneity of particulate nitrate's photochemical reactivity or the consumption of reactive electron donors (Bao et al., 2018). HONO production from the photochemical reactions of particulate nitrate was significantly influenced by ambient environmental conditions (i.e., light intensity and RH). As shown in Fig. 2b, with the increase in light intensity, P_{HONO} gradually increased, with P_{HONO} at a light intensity of 3.85 kW m^{-2} being approximately twice that at 1.50 kW m^{-2}. Previous works have found that the formation of HONO is negligible at low RH levels ($< 5\,\%$) and increases at intermediate RH levels (15 %–75 %), before decreasing at RH levels greater than 90 % (Bao et al., 2018). Here, we found that P_{HONO} climbed to its highest when the RH was around 65 % (Fig. 2c). In this work, the photochemical reactions on different aerosol samples were all conducted under the same environmental conditions (an RH of 65 %, a temperature of 20 °C, and a light intensity of 1.50 kW m^{-2}).

As expected, P_{HONO} increased with particulate nitrate loadings in different sampling locations (Fig. S1 in the Supplement); however, it is interesting to note that P_{HONO} did not increase or somewhat decreased under conditions of very high NO_3^- loading. This phenomenon has also been observed in other works (Ye et al., 2017; Bao et al., 2018). Previous works suggest that this may be attributed to the shadowing effect of particles under heavy aerosol loading conditions on the filters. The particulate nitrate underneath the aerosol filters may receive less UV light because of the presence of particles in the upper layers, inhibiting the photolysis of particulate nitrate (Ye et al., 2017). Assuming that the sampling time of all aerosol filter samples was the same, the aerosol loading on the filters collected under polluted conditions was much higher than that collected under clean conditions. Thus, the reported P_{HONO} values for the aerosol filters collected under polluted ambient conditions would have been underestimated with heavy aerosol particle loading. To verify and quantify the underestimation of P_{HONO} due to the shadowing effect, we collected two sets of filters in Wangdu (set A (daytime and nighttime filters) and set B (all-day filters); Fig. 1b). Theoretically, the all-day set should share the same NO_3^- loading and chemical composition as the sum of the daytime and nighttime filters; thus, the sum of P_{HONO} during daytime ($P_{daytime}^{HONO}$) and that during nighttime ($P_{nighttime}^{HONO}$) should be

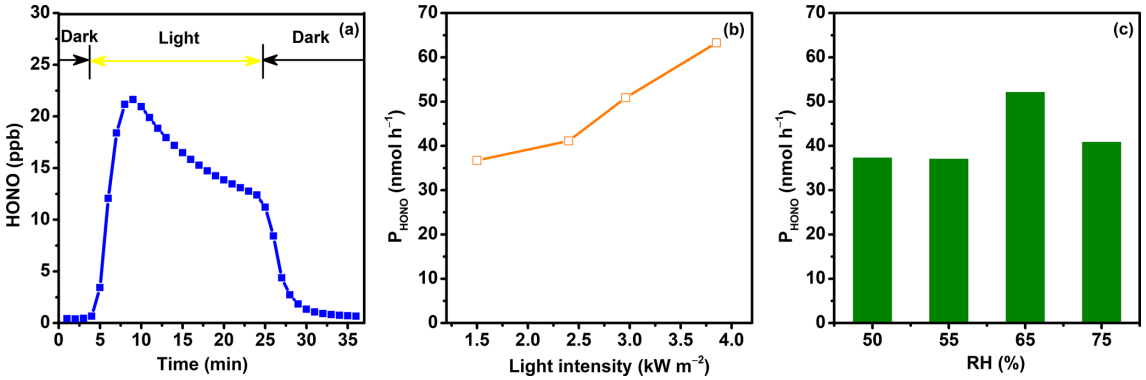

Figure 2. **(a)** Online-measured concentrations of HONO during the light exposure of an aerosol sample collected on 12 June 2023 in Beijing. P_{HONO} as a function of **(b)** light intensity (kW m^{-2}) and **(c)** RH (percentage).

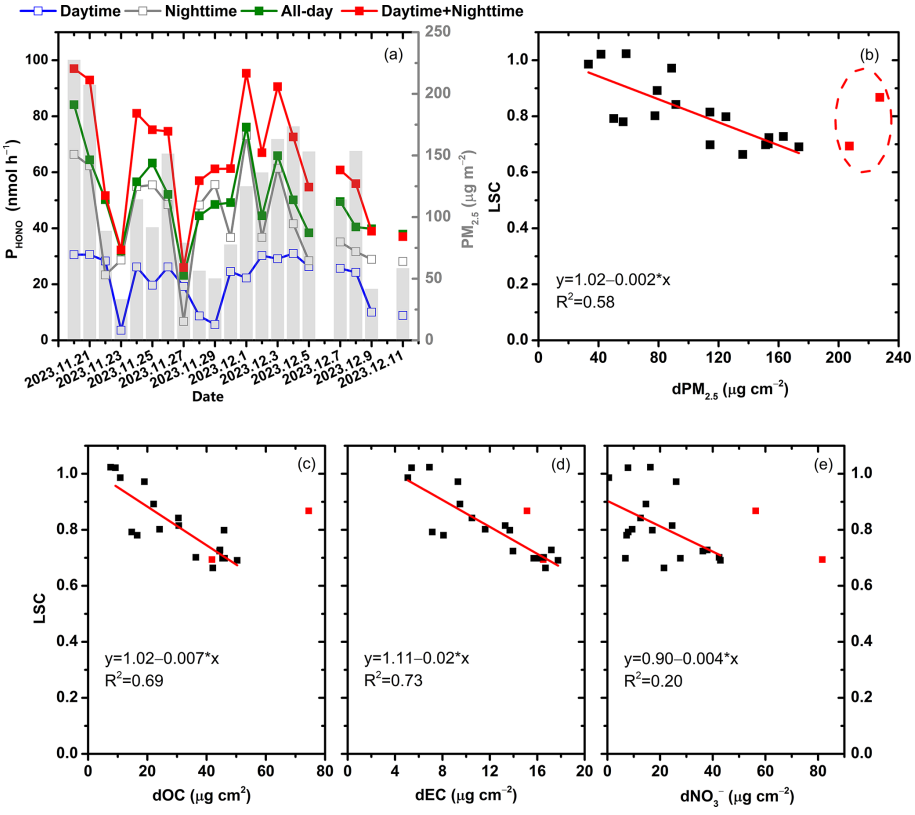

Figure 3. **(a)** Temporal variation in P_{HONO} for aerosol filters collected in Wangdu during daytime, nighttime, and all-day periods from 20 November to 11 December 2023. **(b–e)** Relationships between the light screening coefficient (LSC) and surface concentrations of $PM_{2.5}$ ($dPM_{2.5}$), OC (dOC), EC (dEC), and NO_3^- (dNO_3^-), respectively. The red squares represent aerosol samples with $PM_{2.5}$ surface concentrations higher than 200 μg cm^{-2}.

equal to P_{HONO} during the all-day period ($P^{HONO}_{all\text{-}day}$), without considering the shadowing effect. A total of 20 pairs of comparative photochemical experiments were conducted, and the comparison of P_{HONO} between these two sets of filters is shown in Fig. 3a. We found that the discrepancy between $P^{HONO}_{all\text{-}day}$ and $P^{HONO}_{daytime} + P^{HONO}_{nighttime}$ widened with the increase in surface $PM_{2.5}$ concentration. To quantify the shadowing effect, we introduced a parameter called the "light screening coefficient" (LSC) to describe the decreasing efficiency of light penetration into the particles with increasing $PM_{2.5}$ loadings. The equations are expressed as follows:

$$P^{HONO}_{theory} = P^{HONO}_{daytime} + P^{HONO}_{nighttime}, \quad (3)$$

$$LSC = P^{HONO}_{observed} / P^{HONO}_{corrected} = P^{HONO}_{all\text{-}day} / P^{HONO}_{theory}, \quad (4)$$

where $P^{HONO}_{observed}$ represents the observed production rate of HONO from particulate nitrate photolysis during the photochemical experiment and $P^{HONO}_{corrected}$ represents the corrected value of P_{HONO} after quantifying the shadowing effect. As shown in Fig. 3b, when the $PM_{2.5}$ surface concentration ($dPM_{2.5}$) was low, the LSC was almost equal to 1, indicating that the shadowing effect was negligible. With the increase in $PM_{2.5}$ loading, the value of the LSC declined to less than 65 %. In general, a significant negative correlation existed between the LSC and $dPM_{2.5}$, except when $dPM_{2.5}$ was higher than 200 $\mu g\,cm^{-2}$ (Fig. 3b). In this experiment, we assumed that the daytime and nighttime $PM_{2.5}$ samples were both single-layered. However, with the increase in air pollution, the filters in each pair of comparative experiments may already have exhibited the shadowing effect; thus, the sum of $P^{HONO}_{daytime}$ and $P^{HONO}_{nighttime}$ would have been underestimated. Therefore, when quantifying the shadowing effect, the LSC data with $PM_{2.5}$ loadings higher than 200 $\mu g\,cm^{-2}$ were excluded. Correlations between the LSC and the surface concentrations of major chemical components of $PM_{2.5}$, such as EC (dEC), OC (dOC), and NO_3^- (dNO_3^-), were conducted (Fig. 3c–e). A significant correlation was found between the LSC and the carbonaceous components, especially EC ($R^2 = 0.73$), which was one of the most important light-absorbing species in $PM_{2.5}$, indicating that the shadowing effect was mainly related to the light-absorbing components in $PM_{2.5}$. The relationship between the LSC and dEC was established as follows:

$$\begin{aligned} &dEC > 5.5\,\mu g\,m^{-2}:\ LSC = 1.11\text{–}0.02 \times dEC, \\ &dEC \le 5.5\,\mu g\,m^{-2}:\ LSC = 1. \end{aligned} \quad (5)$$

When $dEC \le 5.5\,\mu g\,m^{-2}$, the shadowing effect can be ignored, and when $dEC > 5.5\,\mu g\,m^{-2}$, P_{HONO} can be corrected using the observed P_{HONO} values and the LSC, which is estimated using the fitting equation with dEC. Previous works have found that heavy loads of carbonaceous particles can turn these filters a dark-brown color. The UV light is unlikely to be transmitted efficiently through the dark layer to the particulate nitrate underneath, thus inhibiting the generation of HONO from the photolysis of particulate nitrate (Ye et al., 2017). In consideration of the potential shadowing effect for the daytime and nighttime filters in each pair of comparative experiments, the observed $P^{HONO}_{daytime}$ and $P^{HONO}_{nighttime}$ values would be underestimated, and the uncertainty in the LSC should be considered at high $PM_{2.5}$ loadings. To evaluate this uncertainty, the observed $P^{HONO}_{daytime}$ and $P^{HONO}_{nighttime}$ values were recalculated and corrected to the theoretical single-layered condition based on Eqs. (4) and (5). As shown in Fig. S2, with the increase in $PM_{2.5}$ surface concentration, the deviations between the LSC and the corrected values enlarged. However, it is noted that the deviation was still lower than 20 % when the $PM_{2.5}$ surface concentration was around 200 $\mu g\,cm^{-2}$. For example, for the aerosol sample collected on 4 December 2023 in Wangdu, the $PM_{2.5}$ surface concentration was 173.57 $\mu g\,cm^{-2}$, and the deviation was 15.74 %, which is acceptable in this work.

3.2 Spatial distribution of and temporal variation in HONO production from particulate nitrate photolysis

There were 158 filter samples collected from five representative cities in China, and the average concentrations of $PM_{2.5}$ and its chemical composition from these filters showed significant spatial characteristics, as shown in Fig. 4. During the sampling period, OM was the most abundant species in $PM_{2.5}$ across most regions, except in the northwestern city of Changji. NO_3^- was the dominant inorganic component in the NCP (Beijing and Wangdu) and central China (Xinxiang), while SO_4^{2-} showed the highest contribution in the PRD region (Guangzhou) and northwestern China (Changji). The values of $J_{NO_3^--HONO}$ for these $PM_{2.5}$ samples were calculated with Eq. (2), with P_{HONO} corrected using Eqs. (4) and (5), and are summarized in Fig. 4 and Table 1. The median and mean (± 1 standard deviation) of the corrected $J_{NO_3^--HONO}$ values were 1.55×10^{-5} and $1.57\,(\pm 2.14) \times 10^{-5}\,s^{-1}$ in Beijing, 1.68×10^{-5} and $1.75\,(\pm 2.83) \times 10^{-5}\,s^{-1}$ in Wangdu, 0.69×10^{-5} and $0.78\,(\pm 0.48) \times 10^{-5}\,s^{-1}$ in Xinxiang, 3.04×10^{-5} and $3.31\,(\pm 1.15) \times 10^{-5}\,s^{-1}$ in Guangzhou, and 0.38×10^{-5} and $0.39\,(\pm 0.25) \times 10^{-5}\,s^{-1}$ in Changji, respectively. The maximum $J_{NO_3^--HONO}$ values for these cities ranged from $0.91 \times 10^{-5}\,s^{-1}$ for Changji to $1.96 \times 10^{-4}\,s^{-1}$ for Wangdu. These values are in a range comparable to values previously reported for aerosol samples, such as 1.22×10^{-5} to $4.84 \times 10^{-4}\,s^{-1}$ for China – reported by Bao et al. (2018) using an RH of 60 %, a temperature of 25 °C, and an irradiation time of 15 min – and 6.2×10^{-6} to $5.0 \times 10^{-4}\,s^{-1}$ (the sum of HONO production and NO_x production, with an average HONO / NO_x production ratio of ~ 2) for the US – reported by Ye et al. (2017) using an RH of 50 %, a temperature of 20 (± 1) °C, and an irradiation time of 10 min. It is interesting to note that the highest average $J_{NO_3^--HONO}$ value was from Guangzhou, which was characterized by the lowest $PM_{2.5}$ and NO_3^- concentrations among the observed cities. As for the other cities with high $PM_{2.5}$ concentrations, such as Changji and Xinxiang, the corrected $J_{NO_3^--HONO}$ values were comparatively low. According to the National Ambient Air Quality Standard of China (GB3095-2012), daily $PM_{2.5}$ averages for Guangzhou can meet the Level-II standard of 75 $\mu g\,m^{-3}$ while exceeding the Level-I standard (35 $\mu g\,m^{-3}$). Here, we defined $PM_{2.5}$-polluted days as days with a daily mean $PM_{2.5}$ value exceeding 35 $\mu g\,m^{-3}$. As shown in Fig. 5, the distribution of the corrected $J_{NO_3^--HONO}$ values on clean days was generally more dispersed and greater than on polluted days, except in the case of Guangzhou. The average value of $J_{NO_3^--HONO}$ for Guangzhou under air-polluted conditions was slightly higher than that under clean conditions and much higher than the values for other cities. Because the

influence of the shadowing effect has been corrected to some degree, the spatial and temporal changes in $J_{NO_3^--HONO}$ presented in this work should be mainly related to the varied chemical and physical properties of $PM_{2.5}$ samples collected from different atmospheric environments.

3.3 Dominant factors controlling $J_{NO_3^--HONO}$

3.3.1 Particulate nitrate

As shown in Table 1, the corrected $J_{NO_3^--HONO}$ values varied with the sampling period and location over a wide range, from $0.16 \times 10^{-5}\,s^{-1}$ for the aerosol sample collected in Changji with $PM_{2.5}$ concentrations higher than $90\,\mu g\,m^{-3}$ to $19.60 \times 10^{-5}\,s^{-1}$ for the aerosol sample collected in Wangdu with $PM_{2.5}$ concentrations lower than $25\,\mu g\,m^{-3}$. Several factors may have contributed to the discrepancy in $J_{NO_3^--HONO}$ in these different aerosol samples, such as particulate nitrate, organic matter, and aerosol acidity.

As shown in Fig. 6, after considering the shadowing effect, the corrected P_{HONO} values generally increased with the amount of particulate nitrate (pNO_3^-; micrograms), but it gradually slowed down under conditions of high particulate nitrate loading, resulting in a rapid decrease in $J_{NO_3^--HONO}$. For example, when NO_3^- concentrations were at a low level (around $0.5\,\mu g\,m^{-3}$) in Wangdu, the value of corrected $J_{NO_3^--HONO}$ was about 30 times higher than that at high NO_3^- concentrations (around $20\,\mu g\,m^{-3}$). Previous works have found that particulate nitrate is associated with matrix components in aerosol samples and that the photolysis reactivity of particulate nitrate is closely associated with the surface catalysis effect (Ye et al., 2017). In such a mechanism, the interaction between particulate nitrate and the substrate can distort the molecular structure of nitrate and increase the absorption cross section. The increases in P_{HONO} with pNO_3^- exposed to light radiation can be fitted by a logarithmic curve under different environmental conditions as follows: $P_{HONO} = \frac{a}{b}\ln(1 + b(pNO_3^-)) + c(pNO_3^-)$, where a, b, and c are the fitting constants (Ye et al., 2017, 2019). Based on this fitting equation, corrected P_{HONO} as a function of pNO_3^- is shown in Fig. 6a. Interestingly, these relationships at different sampling locations showed distinct upward trends. Ye et al. (2019) found that the ratio of a to b was related to the catalytic power of surface reactive sites and the organic matter in the matrix. The much higher ratio of a (4.30) to b (0.06) values fitted for Guangzhou than for other cities, especially Changji ($a = 0.58$; $b = 0.04$), suggests extra catalytic power from organic components in addition to that from surface reactive sites on particulate nitrate. The large deviation in the ratio of a to b among these cities indicates the limitation of predicting P_{HONO} based solely on its relationship with particulate nitrate in different atmospheric environments, and other varying chemical and physical conditions of aerosols should be considered as well.

3.3.2 Organic matter

Organic matter is ubiquitous in the atmosphere and contributes significantly to the total aerosol mass. The selectivity of organic matter that coexists in aerosols is very important for the production of HONO from the photolysis of particulate nitrate (Bao et al., 2018; Ye et al., 2016a; Svoboda et al., 2013; Reeser et al., 2013; Stemmler et al., 2006; Yang et al., 2018; Beine et al., 2006; Wang et al., 2021). As shown in Fig. 7a, corrected P_{HONO} generally increased as the amount of OC in aerosol samples (pOC; µg) went up, although these positive correlations between P_{HONO} and pOC may be due to the moderate correlation between pNO_3^- and pOC ($R^2 = 0.39$; Fig. S3). To eliminate the contribution from particulate nitrate, the dependence of $J_{NO_3^--HONO}$ on the ratio of OC to NO_3^- (OC / NO_3^-) was examined as follows:

$$\text{corrected } J_{NO_3^--HONO} = 0.74 \times (OC/NO_3^-) + 0.08. \quad (6)$$

As shown in Fig. 7b, a significant linear correlation between corrected $J_{NO_3^--HONO}$ and OC / NO_3^- was found, with an R^2 value of 0.86. In general, high corrected $J_{NO_3^--HONO}$ values were mostly associated with high OC / NO_3^- ratios for aerosol samples collected in clean areas, such as Guangzhou, where the average $PM_{2.5}$ level was the lowest (Fig. 7c). Low corrected $J_{NO_3^--HONO}$ values were mostly associated with low OC / NO_3^- ratios. Generally, cities with higher $PM_{2.5}$ levels, such as Changji and Xinxiang, have lower OC / NO_3^- ratios; however, we found an exception – Wangdu, a rural site in the North China Plain, where $PM_{2.5}$ levels were high but dominated by OM, mainly due to local residential coal combustion (Liu et al., 2016; Li et al., 2024; Liu et al., 2017). As shown in Fig. 5b, the OC / NO_3^- ratio on clean days was generally higher than that observed under polluted conditions. Interestingly, unlike in other cities, the OC / NO_3^- ratio in Guangzhou increased under polluted conditions, consistent with the correspondingly higher corrected $J_{NO_3^--HONO}$ value. Guangzhou is located in the PRD region and is characterized by $PM_{2.5}$ containing large fractions of OM, due to large emissions of VOCs from numerous manufacturing industries and transport-related sources (Zheng et al., 2009). Here, water-soluble organic carbon (WSOC) is the dominant component in organic aerosols ($WSOC / OC = 0.63$) (Chang et al., 2019). It is reported that organic compounds on the surface may act as photosensitizers in the photolysis of particulate nitrate (Gen et al., 2022; Handley et al., 2007; Cao et al., 2022; Wang et al., 2021). The association of particulate nitrate with organic matter may distort its molecular structure and enhance the absorption cross section, resulting in a significant enhancement of the photochemical production of HONO. Organic matter can also act as a hydrogen donor, directly transferring hydrogen from organic H donors to NO_2 to form HONO (Gen et al., 2022). Therefore, we suggest that the gradually increasing role of organic matter in $PM_{2.5}$ in China should be of great concern.

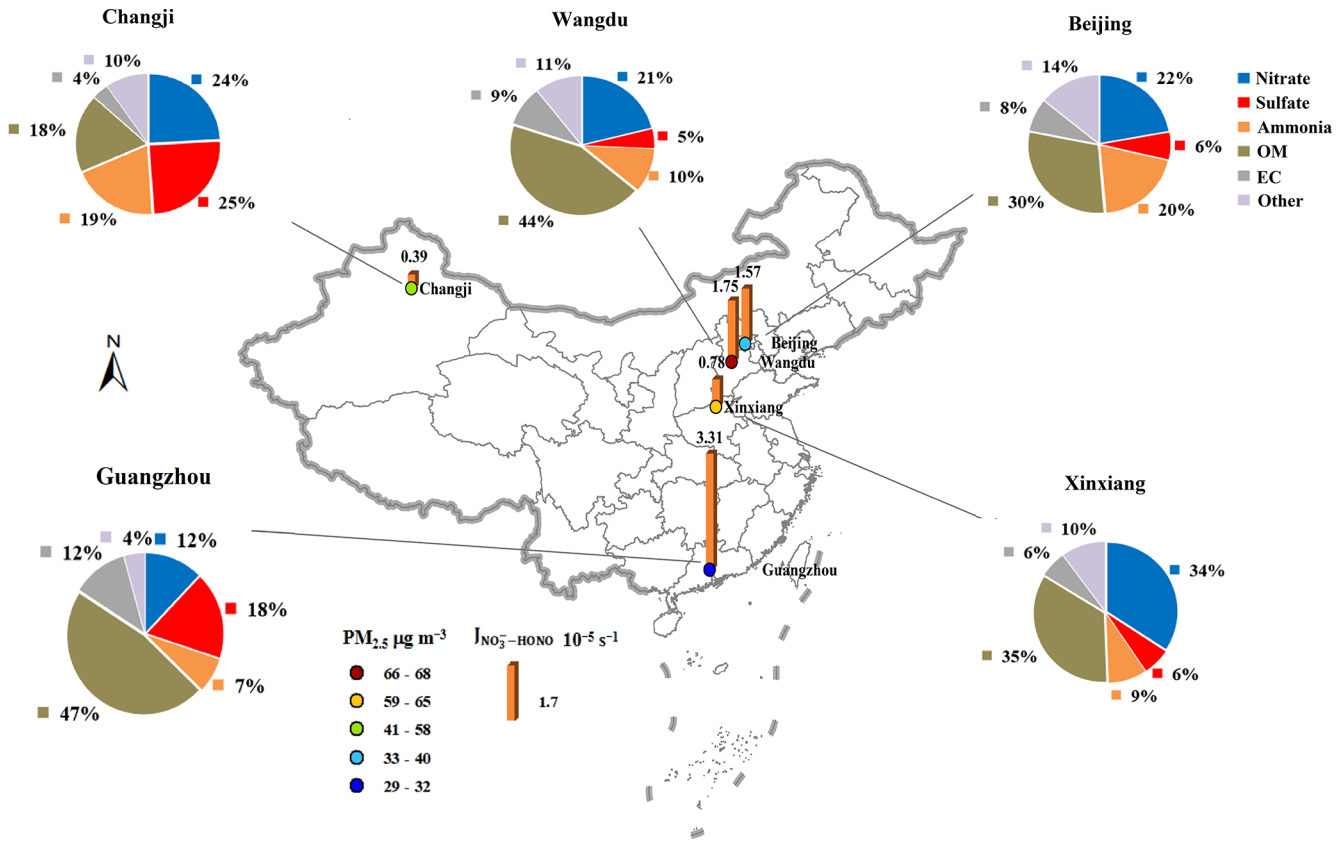

Figure 4. Spatial distribution of the average $J_{NO_3^--HONO}$ values, the $PM_{2.5}$ loading, and the chemical composition of the aerosol filters collected from the five representative cities in China during the observation period.

3.3.3 Other factors

The acidic proton may play an important role in the photochemical production of HONO and affect the release of photolysis products (Bao et al., 2018; Scharko et al., 2014). Scharko et al. (2014) found that gaseous HONO production from nitrate photolysis was highest at the lowest level of aerosol acidity (with a pH of ~ 2), decreased with pH, and reached almost zero at pH values higher than 4. In this work, the estimated pH of these aerosol samples was in the range of 1.83–3.46 (using the Extended Aerosol Inorganics Model (E-AIM); Shi et al., 2021; Wexler and Clegg, 2002; Clegg et al., 1998), with detailed information provided in the Supplement. As shown in Fig. S4, however, the correlation between pH and $J_{NO_3^--HONO}$ was weak, indicating that pH was an important factor but not the key one driving the spatial differences in $J_{NO_3^--HONO}$ in this work. Noting that halide ions, such as chloride ions (Cl^-), may lead to the enhancement of surface nitrate anions and promote nitrate photolysis (Gen et al., 2022; R. Zhang et al., 2020), we also plotted $J_{NO_3^--HONO}$ against the molar ratio of Cl^- to NO_3^- (Cl^- / NO_3^-), as shown in Fig. 8a. Even though Guangzhou is a southern coastal city, the sampling site in this work was far away (> 50 km) from the South China Sea. Additionally, during the observation period, the aerosol collected in Guangzhou was more representative of inland aerosol than marine aerosol, with air parcels usually coming from inland directions (Fig. 8b) and the ratio of Cl^- to NO_3^- (0.02) being much lower than that for fresh sea spray aerosol (> 1.0) (Xiao et al., 2017; Pipalatkar et al., 2014; Atzei et al., 2019; Wang et al., 2019). Therefore, we suggest that halide ions were not the determining factor for the high $J_{NO_3^--HONO}$ value in Guangzhou and that the exact role of halide ions in HONO formation through the photolysis of particulate nitrate requires further investigation.

3.4 Environmental implication

The determined $J_{NO_3^--HONO}$ values were closely associated with the aerosol's chemical and physical characteristics, especially the coexisting organic components, and were distributed around the curve as expressed by Eq. (6). This is the first effort to explore the photolysis of particulate nitrate in aerosol samples collected from different typical regions of China. The enhanced formation of HONO from the photolysis of particulate nitrate can contribute significantly to the atmospheric oxidation capacity. To assess the photolysis of

Table 1. $PM_{2.5}$, NO_3^-, and OC concentrations, the ratio of OC to NO_3^- (OC/NO_3^-), corrected $J_{NO_3^-\text{–HONO}}$, and S_{HONO} (the noontime source strength of HONO) across five representative cities in China under different air conditions during the sampling period.

Site	Air condition	$PM_{2.5}$ ($\mu g\,m^{-3}$)	NO_3^- ($\mu g\,m^{-3}$)	OC ($\mu g\,m^{-3}$)	OC/NO_3^-	Corrected $J_{NO_3^-\text{–HONO}}$ ($10^{-5}\,s^{-1}$)[a]	S_{HONO} ($10^{-5}\,mol\,h^{-1}\,m^{-2}$)[b]	S_{HONO} ($ppbv\,h^{-1}$)[c]
Beijing	Clean	19.71 ± 8.65	3.15 ± 2.34	3.89 ± 2.13	2.25 ± 3.03	2.01 ± 2.44	0.15 ± 0.07	0.03 ± 0.02
	Polluted	72.56 ± 23.78	19.71 ± 10.72	12.62 ± 2.18	0.87 ± 0.62	0.61 ± 0.30	0.38 ± 0.11	0.09 ± 0.02
	Whole – min	4.32	0.08	1.07	0.32	0.21	0.04	0.01
	Whole – max	102.64	32.90	15.95	12.82	11.06	0.57	0.13
	Whole – mean	32.92	7.29	6.07	1.85	1.57	0.22	0.05
Changji	Clean	20.39 ± 6.00	3.05 ± 1.75	3.61 ± 1.08	1.66 ± 1.11	0.65 ± 0.18	0.07 ± 0.03	0.02 ± 0.01
	Polluted	80.49 ± 39.54	20.59 ± 4.74	8.35 ± 2.97	0.44 ± 0.08	0.21 ± 0.03	0.16 ± 0.04	0.04 ± 0.01
	Whole – min	14.45	0.88	2.69	0.28	0.16	0.03[d]	0.01[d]
	Whole – max	169.35	28.28	14.34	3.65	0.91	0.22	0.05
	Whole – mean	57.37	13.84	6.53	0.91	0.39	0.13	0.03
Guangzhou	Clean	25.62 ± 6.08	3.29 ± 1.68	6.89 ± 2.21	2.72 ± 1.79	3.25 ± 1.28	0.36 ± 0.15	0.08 ± 0.03
	Polluted	40.32 ± 2.23	4.38 ± 1.30	13.82 ± 1.34	3.35 ± 0.86	3.53 ± 0.61	0.59 ± 0.15	0.13 ± 0.03
	Whole – min	14.77	0.85	3.67	0.82	1.37	0.17	0.04
	Whole – max	42.74	6.63	15.62	8.05	5.83	0.75	0.17
	Whole – mean	29.12	3.55	8.54	2.87	3.31	0.41	0.09
Wangdu	Clean	22.16 ± 7.66	3.29 ± 2.59	5.36 ± 2.38	4.79 ± 6.46	3.80 ± 5.10	0.20 ± 0.09	0.04 ± 0.02
	Polluted	83.53 ± 30.47	18.06 ± 12.48	23.23 ± 9.62	1.88 ± 1.67	1.09 ± 0.87	0.50 ± 0.15	0.11 ± 0.03
	Whole – min	10.67	0.24	2.72	0.22	0.23	0.06	0.01
	Whole – max	173.45	60.28	63.07	22.06	19.60	0.88[e]	0.20[e]
	Whole – mean	68.38	14.41	18.82	2.60	1.75	0.42	0.10
Xinxiang	Clean	23.53 ± 5.45	4.35 ± 1.41	5.69 ± 2.46	1.37 ± 0.61	1.28 ± 0.49	0.21 ± 0.07	0.05 ± 0.02
	Polluted	68.98 ± 33.43	24.87 ± 21.5	14.63 ± 4.41	0.87 ± 0.45	0.62 ± 0.35	0.40 ± 0.12	0.09 ± 0.03
	Whole – min	18.32	2.37	2.33	0.30	0.19	0.09	0.02
	Whole – max	143.10	73.47	22.06	2.02	1.96	0.59	0.13
	Whole – mean	57.62	19.74	12.40	0.99	0.78	0.35	0.08

[a] Represents the photolysis rate constant of particulate nitrate leading to HONO production, considering the influence of the shadowing effect.
[b, c] Represents the noontime source strength of HONO through the photolysis of particulate nitrate, with units of $10^{-5}\,mol\,h^{-1}\,m^{-2}$ or $ppbv\,h^{-1}$.
[d, e] Represents the minimum and maximum values of S_{HONO} during the observation period.

particulate nitrate as a daytime HONO source, the noontime source strength of HONO (S_{HONO}) through this mechanism in the air column within the planetary boundary layer can be calculated using the following equation (Ye et al., 2017):

$$S_{HONO}\,(10^{-5}\,mol\,h^{-1}\,m^{-2}) = 0.67 \times NO_3^-(\mu mol\,m^{-3}) \times 10^{-6} \times J_{NO_3^-\text{–HONO}} \times BLH \times 3600, \quad (7)$$

or

$$S_{HONO}\,(ppbv\,h^{-1}) = 0.67 \times NO_3^-(ppbv) \times J_{NO_3^-\text{–HONO}} \times 3600, \quad (8)$$

where BLH refers to the boundary mixing height (meters). Here, we assume a typical BLH of 1000 m. Based on the daily measured NO_3^- and corrected $J_{NO_3^-\text{–HONO}}$ values for each city, the S_{HONO} values derived from Eq. (7) or Eq. (8) during the observation period are shown in Table 1. It was found that, even though $J_{NO_3^-\text{–HONO}}$ on polluted days was much lower than that on clean days, due to the apparent higher NO_3^- concentration, the corresponding S_{HONO} values were about twice the average on clean days. The calculated S_{HONO} values ranged from 0.03×10^{-5} to $0.88 \times 10^{-5}\,mol\,h^{-1}\,m^{-2}$ (0.01–0.2 $ppbv\,h^{-1}$), with a mean value of $0.36 \times 10^{-5}\,mol\,h^{-1}\,m^{-2}$ (0.08 $ppbv\,h^{-1}$), comparable to or higher than that for other HONO sources (Bhattarai et al., 2019; Wang et al., 2023; Ye et al., 2017). For example, the soil HONO emission flux was measured to be in the range of 1.81×10^{-6} to $4.55 \times 10^{-6}\,mol\,h^{-1}\,m^{-2}$ in soil not treated with nitrogen fertilizer (Bhattarai et al., 2019). The mean value of S_{HONO} during the observation period was highest in Wangdu ($0.42 \times 10^{-5}\,mol\,h^{-1}\,m^{-2}$ and 0.10 $ppbv\,h^{-1}$) and Guangzhou ($0.41 \times 10^{-5}\,mol\,h^{-1}\,m^{-2}$ and 0.09 $ppbv\,h^{-1}$), followed by Xinxiang ($0.35 \times 10^{-5}\,mol\,h^{-1}\,m^{-2}$ and 0.08 $ppbv\,h^{-1}$), Beijing ($0.22 \times 10^{-5}\,mol\,h^{-1}\,m^{-2}$ and 0.05 $ppbv\,h^{-1}$), and Changji ($0.13 \times 10^{-5}\,mol\,h^{-1}\,m^{-2}$ and 0.03 $ppbv\,h^{-1}$). Even though the $PM_{2.5}$ and NO_3^- concentrations were lowest in Guangzhou, S_{HONO} was much higher here than in other cities with air pollution. It should be noted that the S_{HONO} value calculated with the daily changing NO_3^- and $J_{NO_3^-\text{–HONO}}$ values from this work was much lower than the value reported by Bao et al. (2018) (0.78 $ppbv\,h^{-1}$), who applied the average NO_3^- value (6.64 $\mu g\,m^{-3}$ (2.62 ppbv)) and the $J_{NO_3^-\text{–HONO}}$ range (1.22×10^{-5} to $4.84 \times 10^{-4}\,s^{-1}$) to simulate S_{HONO} (0.12–4.57 $ppbv\,h^{-1}$). Other works, such as Fu et al. (2019) and

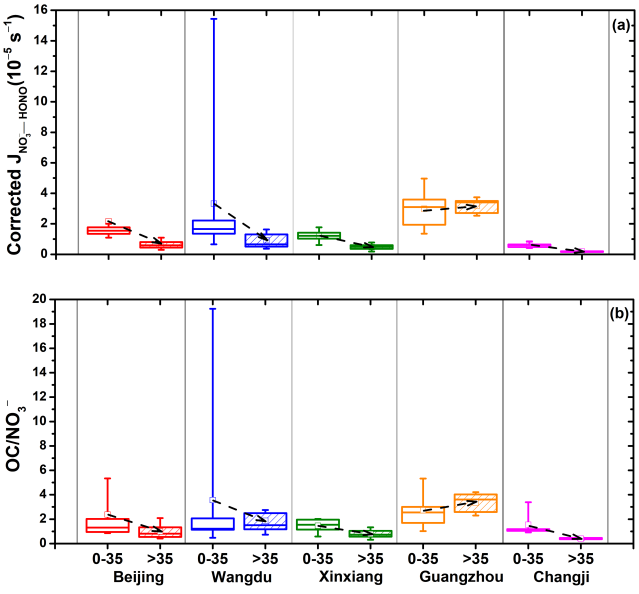

Figure 5. **(a)** Average corrected $J_{NO_3^-\text{–HONO}}$ values and **(b)** the ratio of OC to NO_3^- under different air conditions in five representative cities. The boxes represent the 25th to 75th percentiles; the horizon lines represent the medians; the hollow squares represent the means; and the bottom and top whiskers represent the 10th and 90th percentiles, respectively.

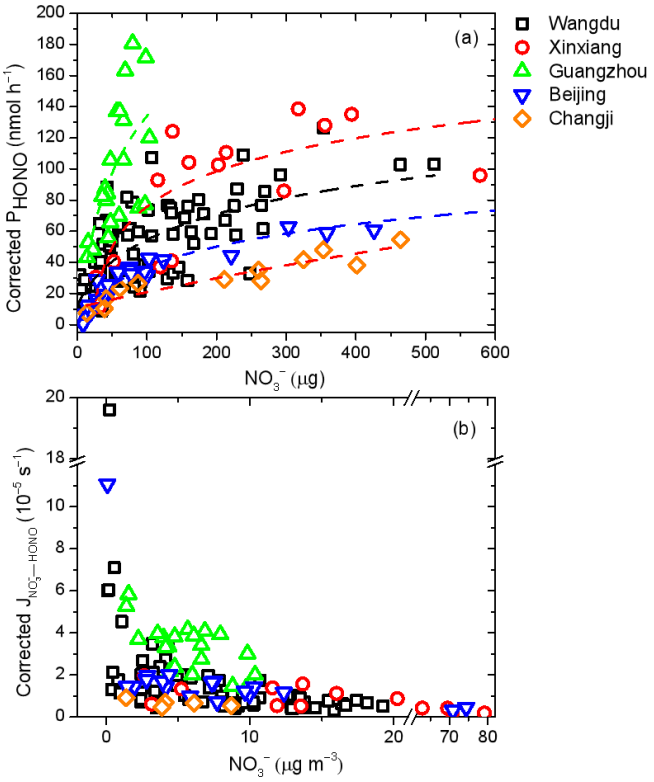

Figure 6. Relationships between **(a)** corrected P_{HONO} and particulate nitrate loading and **(b)** corrected $J_{NO_3^-\text{–HONO}}$ and particulate nitrate concentration across different sampling locations. The dashed lines in panel **(a)** represent the best fits to the data for the fitting equation with respect to the aerosol samples from Guangzhou ($a = 4.30$; $b = 0.06$; $c = 1 \times 10^{-6}$; $R^2 = 0.42$), Wangdu ($a = 2.54$; $b = 0.11$; $c = 1 \times 10^{-6}$; $R^2 = 0.50$), Beijing ($a = 1.51$; $b = 0.06$; $c = 1 \times 10^{-6}$; $R^2 = 0.91$), Xinxiang ($a = 2.28$; $b = 0.06$; $c = 1 \times 10^{-6}$; $R^2 = 0.47$), and Changji ($a = 0.58$; $b = 0.04$; $c = 1 \times 10^{-6}$; $R^2 = 0.86$).

Gu et al. (2022a), applied the mean value of $J_{NO_3^-\text{–HONO}}$ (8.3×10^{-5} s^{-1}) and the observed NO_3^- concentration to calculate S_{HONO}. However, due to the significant decrease in $J_{NO_3^-\text{–HONO}}$ along with the increase in NO_3^-, the S_{HONO} values calculated with mean NO_3^- or $J_{NO_3^-\text{–HONO}}$ values are largely overestimated, thus directly influencing the identification of HONO sources. For example, $J_{NO_3^-\text{–HONO}}$ was at its highest in Wangdu on 23 November 2023, with a value of 19.6×10^{-5} s^{-1}, while the corresponding NO_3^- concentration was low (0.39 μg m^{-3}). If the average NO_3^- concentration (12.53 μg m^{-3}, equivalent to 4.53 ppbv) and the maximum $J_{NO_3^-\text{–HONO}}$ value were applied, the determined S_{HONO} value would be 9.56×10^{-5} mol h^{-1} m^{-2} (2.14 ppbv h^{-1}), which is about 30 times higher than the actual result (0.07 ppbv h^{-1}). Therefore, we suggest estimating S_{HONO} with the observed concentration of NO_3^- and the $J_{NO_3^-\text{–HONO}}$ value derived from the parameterization equation with OC / NO_3^-, thereby reducing the large uncertainties and improving estimations of the HONO budget.

On the basis of daily average concentrations of NO_3^- and OC extracted from a Chinese high-resolution $PM_{2.5}$ component simulation concentration dataset (the CAQRA-aerosol dataset (15 km × 15 km); https://www.capdatabase.cn, last access: 28 May 2024) (Kong et al., 2024), $J_{NO_3^-\text{–HONO}}$ and S_{HONO} can be estimated using Eqs. (6) and (8), respectively. As shown in Fig. 9, significant spatiotemporal changes in NO_3^-, OC, $J_{NO_3^-\text{–HONO}}$, and S_{HONO} were demonstrated in the fall–winter seasons from 2013 to 2022 in China. The high $J_{NO_3^-\text{–HONO}}$ values were concentrated in the clean environments (e.g., the Tibetan Plateau region, the southern Xinjiang basin, the Yunnan–Guizhou Plateau, and the Sichuan Basin), followed by the air-polluted regions (e.g., the NCP, the Fenhe–Weihe basin, northeastern China, and the PRD). From 2013 to 2022, with OC decreasing significantly and NO_3^- staying stable or even increasing, $J_{NO_3^-\text{–HONO}}$ showed a downward trend in most regions. Although the $J_{NO_3^-\text{–HONO}}$ values for polluted regions were comparatively lower than those for clean environments, the higher values of S_{HONO} were mostly distributed in these polluted regions due to the much higher NO_3^- concentration. However, it should be noted that the photolysis of particulate nitrate contributed only a small fraction to the needed daytime HONO source in these polluted regions, with values such as 1.26–3.82 ppbv h^{-1} for the cities in the North China Plain (Hou et

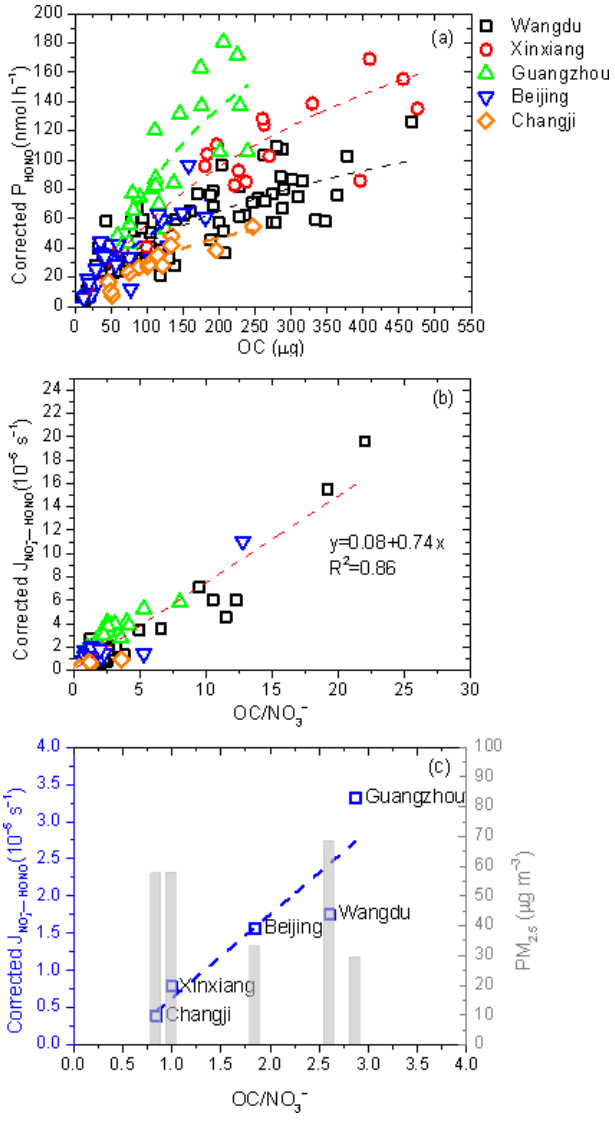

Figure 7. Relationships between **(a)** corrected P_{HONO} and OC loadings; **(b)** corrected $J_{NO_3^--HONO}$ and OC / NO_3^-; and **(c)** average corrected $J_{NO_3^--HONO}$ values, $PM_{2.5}$, and OC / NO_3^- during the sampling period across the five representative cities.

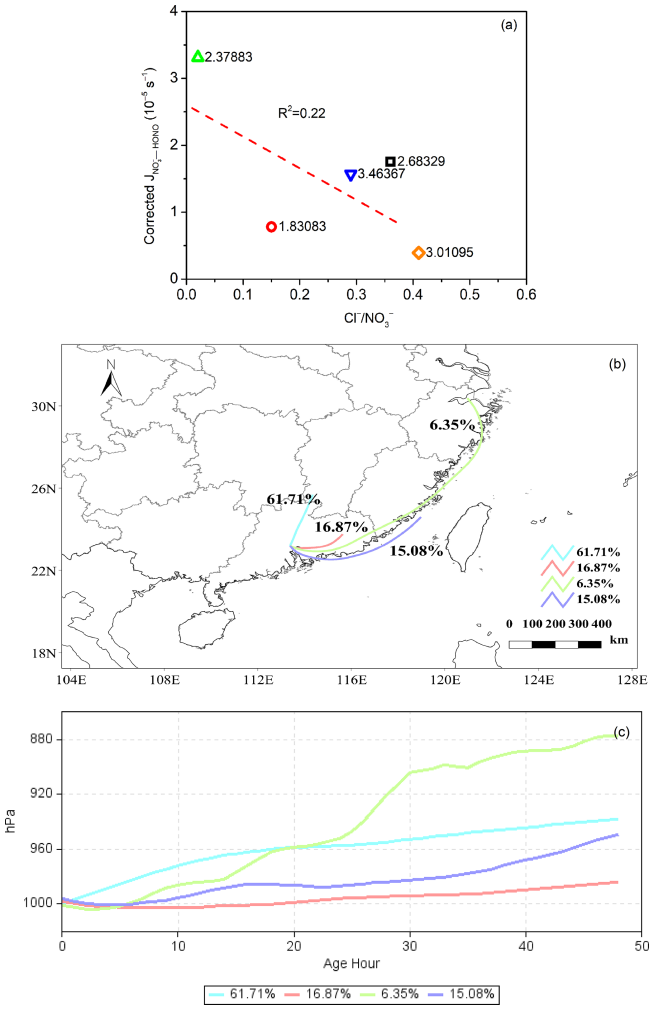

Figure 8. **(a)** Relationship between average corrected $J_{NO_3^--HONO}$ values and Cl$^-$ / NO_3^- across different sampling locations and **(b, c)** a back-trajectory cluster analysis for Guangzhou during the sampling period.

al., 2016; Wang et al., 2017; Lian et al., 2022; Li et al., 2018), 0.75 ppbv h^{-1} for western China (Huang et al., 2017), and 0.77–4.90 ppbv h^{-1} for southern China (Li et al., 2012; Su et al., 2008). We note that uncertainties still exist in our simulations. Given the paucity of field measurements of HONO production from aerosol samples obtained in clean environments, the deviation of $J_{NO_3^--HONO}$ derived from the parameterization in this work may be large in these regions. Additionally, the concentrations of NO_3^- and OC extracted from the CAQRA-aerosol dataset with regard to clean environments were around the mean deviation level. Therefore, more field observations and simulation experiments should be conducted in these clean regions in the future to enrich and improve the parametric equations of $J_{NO_3^--HONO}$ and to further evaluate the contribution of nitrate photolysis to the formation of HONO in different regions of China.

4 Conclusions

This study systematically analyzed, for the first time, the production of HONO from the photolysis of particulate nitrate in $PM_{2.5}$ samples from multiple sites across China, shedding light on the contribution of this photolysis process to daytime HONO sources in different environments. A total of 20 pairs of comparative photochemical experiments were conducted in Wangdu to evaluate and quantify the shadowing effect. We found that the corrected $J_{NO_3^--HONO}$ values varied with the sampling period and location over a wide range, from 0.16×10^{-5} to 19.60×10^{-5} s^{-1}. The coexisting or-

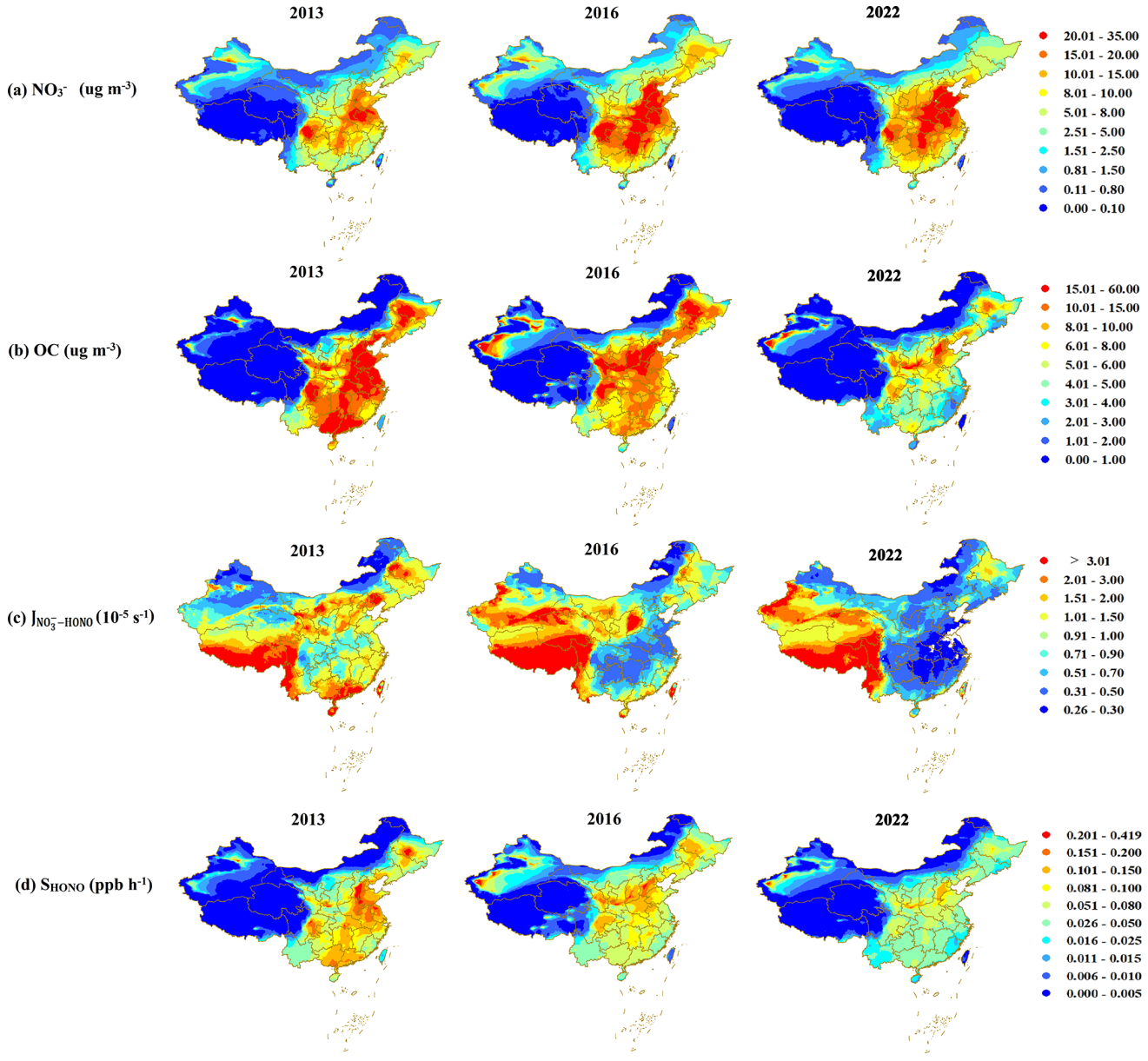

Figure 9. Spatial distributions of daily average **(a)** NO_3^-, **(b)** OC, **(c)** $J_{NO_3^-–HONO}$, and **(d)** S_{HONO} levels from 15 November to 15 December for the years 2013, 2016, and 2022 in China. The daily average concentrations of NO_3^- and OC were extracted from a Chinese high-resolution $PM_{2.5}$ component simulation concentration dataset (Kong et al., 2024). The $J_{NO_3^-–HONO}$ and S_{HONO} values estimated in this work were derived under the same environmental conditions (an RH of 65 %, a temperature of 20 °C, and a light intensity of 150 kW m^{-2}); thus, they are more representative of the potential for HONO production than of the actual values for the real ambient environment.

ganic components in $PM_{2.5}$ can promote the photolysis of particulate nitrate, with higher $J_{NO_3^-–HONO}$ values generally associated with a higher OC / NO_3^- ratio. Considering the logarithmic decrease in $J_{NO_3^-–HONO}$ with increased NO_3^-, we suggest that S_{HONO} should be calculated using $J_{NO_3^-–HONO}$ derived from the parameterization equation with OC / NO_3^-, instead of an average value. The photolysis of particulate nitrate can become a potential daytime HONO source in southern urban cities, such as Guangzhou, which are characterized by large VOC emissions and the enhanced formation of secondary particulate organic matter. Our work provides an important reference for research in other areas in the world with aerosol samples containing a high proportion of organic components, such as the United States (Hass-Mitchell et al., 2024) and Europe (Bressi et al., 2021). It is important to note that the filter samples collected in this work may not cover all representative environments in China, especially background

sites. More field observations and simulation experiments are needed in the future to better constrain the parameterization and mechanism of particulate nitrate photolysis.

Data availability. The data used in this paper can be provided upon request from the corresponding author.

Supplement. The supplement related to this article is available online at: https://doi.org/10.5194/acp-24-13183-2024-supplement.

Author contributions. JW, BL, and KZ conceived the study and designed the experiments. JW, BL, JG, CC, LW, YueZ, JL, YuzZ, and XD analyzed the data. JW and BL prepared the paper, and all the coauthors helped improve it.

Competing interests. The contact author has declared that none of the authors has any competing interests.

Disclaimer. Publisher's note: Copernicus Publications remains neutral with regard to jurisdictional claims made in the text, published maps, institutional affiliations, or any other geographical representation in this paper. While Copernicus Publications makes every effort to include appropriate place names, the final responsibility lies with the authors. Regarding the maps used in this paper, please note that Figs. 1, 4, and 9, as well as the key figure, contain disputed territories.

Acknowledgements. We acknowledge the high-resolution simulation dataset of $PM_{2.5}$ chemical composition in Chinese from 2013 to 2020, which was supported by the National Natural Science Foundation of China (grant no. 92044303; https://www.capdatabase.cn).

Financial support. This research has been supported by the Central Level, Scientific Research Institutes for Basic R&D Special Fund Business, China (grant no. 2022YSKY-26), and the National Key Research and Development Program of China (grant no. 2022YFC3701100).

Review statement. This paper was edited by Benjamin A Nault and reviewed by two anonymous referees.

References

Ammann, M., Kalberer, M., Jost, D. T., Tobler, L., Rössler, E., Piguet, D., Gäggeler, H. W., and Baltensperger, U.: Heterogeneous production of nitrous acid on soot in polluted air masses, Nature, 395, 157–160, https://doi.org/10.1038/25965, 1998.

Andersen, S. T., Carpenter, L. J., Reed, C., Lee, J. D., Chance, R., Sherwen, T., Vaughan, A. R., Stewart, J., Edwards, P. M., Bloss, W. J., Sommariva, R., Crilley, L. R., Nott, G. J., Neves, L., Read, K., Heard, D. E., Seakins, P. W., Whalley, L. K., Boustead, G. A., Fleming, L. T., Stone, D., and Fomba, K. W.: Extensive field evidence for the release of HONO from the photolysis of nitrate aerosols, Sci. Adv., 9, eadd6266, https://doi.org/10.1126/sciadv.add6266, 2023.

Atzei, D., Fermo, P., Vecchi, R., Fantauzzi, M., Comite, V., Valli, G., Cocco, F., and Rossi, A.: Composition and origin of $PM_{2.5}$ in Mediterranean Countryside, Environ. Pollut., 246, 294–302, https://doi.org/10.1016/j.envpol.2018.12.012, 2019.

Bao, F., Li, M., Zhang, Y., Chen, C., and Zhao, J.: Photochemical aging of Beijing urban $PM_{2.5}$: HONO production, Environ. Sci. Technol., 52, 6309–6316, https://doi.org/10.1021/acs.est.8b00538, 2018.

Bao, F., Jiang, H., Zhang, Y., Li, M., Ye, C., Wang, W., Ge, M., Chen, C., and Zhao, J.: The key role of sulfate in the photochemical renoxification on real $PM_{2.5}$, Environ. Sci. Technol., 54, 3121–3128, https://doi.org/10.1021/acs.est.9b06764, 2020.

Beine, H. J., Amoroso, A., Dominé, F., King, M. D., Nardino, M., Ianniello, A., and France, J. L.: Surprisingly small HONO emissions from snow surfaces at Browning Pass, Antarctica, Atmos. Chem. Phys., 6, 2569–2580, https://doi.org/10.5194/acp-6-2569-2006, 2006.

Bhattarai, H. R., Liimatainen, M., Nykänen, H., Kivimäenpää, M., Martikainen, P. J., and Maljanen, M.: Germinating wheat promotes the emission of atmospherically significant nitrous acid (HONO) gas from soils, Soil Biol. Biochem., 136, 107518, https://doi.org/10.1016/j.soilbio.2019.06.014, 2019.

Bressi, M., Cavalli, F., Putaud, J. P., Fröhlich, R., Petit, J. E., Aas, W., Äijälä, M., Alastuey, A., Allan, J. D., Aurela, M., Berico, M., Bougiatioti, A., Bukowiecki, N., Canonaco, F., Crenn, V., Dusanter, S., Ehn, M., Elsasser, M., Flentje, H., Graf, P., Green, D. C., Heikkinen, L., Hermann, H., Holzinger, R., Hueglin, C., Keernik, H., Kiendler-Scharr, A., Kubelová, L., Lunder, C., Maasikmets, M., Makeš, O., Malaguti, A., Mihalopoulos, N., Nicolas, J. B., O'Dowd, C., Ovadnevaite, J., Petralia, E., Poulain, L., Priestman, M., Riffault, V., Ripoll, A., Schlag, P., Schwarz, J., Sciare, J., Slowik, J., Sosedova, Y., Stavroulas, I., Teinemaa, E., Via, M., Vodička, P., Williams, P. I., Wiedensohler, A., Young, D. E., Zhang, S., Favez, O., Minguillón, M. C., and Prevot, A. S. H.: A European aerosol phenomenology – 7: High-time resolution chemical characteristics of submicron particulate matter across Europe, Atmos. Environ. X, 10, 107518, https://doi.org/10.1016/j.aeaoa.2021.100108, 2021.

Cao, Y., Ma, Q., Chu, B., and He, H.: Homogeneous and heterogeneous photolysis of nitrate in the atmosphere: state of the science, current research needs, and future prospects, Front. Env. Sci. Eng., 17, 48, https://doi.org/10.1007/s11783-023-1648-6, 2022.

Chang, D., Wang, Z., Guo, J., Li, T., Liang, Y., Kang, L., Xia, M., Wang, Y., Yu, C., Yun, H., Yue, D., and Wang, T.: Characterization of organic aerosols and their precursors in southern China during a severe haze episode in January 2017, Sci. Total. Environ., 691, 101–111, https://doi.org/10.1016/j.scitotenv.2019.07.123, 2019.

Cheng, C., Yang, S., Yuan, B., Pei, C., Zhou, Z., Mao, L., Liu, S., Chen, D., Cheng, X., Li, M., Shao, M., and Zhou, Z.: The significant contribution of nitrate to a severe haze event in the

winter of Guangzhou, China, Sci. Total. Environ., 909, 168582, https://doi.org/10.1016/j.scitotenv.2023.168582, 2024.

Clegg, S. L., Brimblecombe, P., and Wexler, A. S.: Thermodynamic Model of the System H^+-NH_4^+-Na^+-SO_4^{2-}-NO_3^--Cl^--H_2O at 298.15 K, J. Phy. Chem. A, 102, 2155–2171, https://doi.org/10.1021/jp973043j, 1998.

Donaldson, M. A., Bish, D. L., and Raff, J. D.: Soil surface acidity plays a determining role in the atmospheric-terrestrial exchange of nitrous acid, P. Natl. Acad. Sci. USA, 52, 18472–18477, https://doi.org/10.1073/pnas.1418545112, 2014.

Finlayson-Pitts, B. J. and Pitts Jr., J. N.: Chemistry of the upper and lower atmosphere: theory, experiments, and applications, Academic Press, San Diego, CA, xxii+969 pp., ISBN 0-12-257060-x, 2000.

Fu, X., Wang, T., Zhang, L., Li, Q., Wang, Z., Xia, M., Yun, H., Wang, W., Yu, C., Yue, D., Zhou, Y., Zheng, J., and Han, R.: The significant contribution of HONO to secondary pollutants during a severe winter pollution event in southern China, Atmos. Chem. Phys., 19, 1–14, https://doi.org/10.5194/acp-19-1-2019, 2019.

Gelencsér, A., Hoffer, A., Kiss, G., Tombácz, E., Kurdi, R., and Bencze, L.: In-situ formation of light-absorbing organic matter in cloud water, J. Atmos. Chem., 45, 25–33, https://doi.org/10.1023/A:1024060428172, 2003.

Gen, M., Liang, Z., Zhang, R., Go Mabato, B. R., and Chan, C. K.: Particulate nitrate photolysis in the atmosphere, Environ. Sci.-Atmos., 2, 111–127, https://doi.org/10.1039/d1ea00087j, 2022.

Gu, R., Shen, H., Xue, L., Wang, T., Gao, J., Li, H., Liang, Y., Xia, M., Yu, C., Liu, Y., and Wang, W.: Investigating the sources of atmospheric nitrous acid (HONO) in the megacity of Beijing, China, Sci. Total Environ., 812, 152270, https://doi.org/10.1016/j.scitotenv.2021.152270, 2022a.

Gu, R., Wang, W., Peng, X., Xia, M., Zhao, M., Zhang, Y., Wang, Y., Liu, Y., Shen, H., Xue, L., Wang, T., and Wang, W.: Nitrous acid in the polluted coastal atmosphere of the South China Sea: Ship emissions, budgets, and impacts, Sci. Total. Environ., 826, 153692, https://doi.org/10.1016/j.scitotenv.2022.153692, 2022b.

Handley, S. R., Clifford, D., and Donaldson, D. J.: Photochemical loss of nitric acid on organic films: a possible recycling mechanism for NO_x, Environ. Sci. Technol., 41, 3898–3903, https://doi.org/10.1021/es062044z, 2007.

Hass-Mitchell, T., Joo, T., Rogers, M., Nault, B. A., Soong, C., Tran, M., Seo, M., Machesky, J. E., Canagaratna, M., Roscioli, J., Claflin, M. S., Lerner, B. M., Blomdahl, D. C., Misztal, P. K., Ng, N. L., Dillner, A. M., Bahreini, R., Russell, A., Krechmer, J. E., Lambe, A., and Gentner, D. R.: Increasing contributions of temperature-dependent oxygenated organic aerosol to summertime particulate matter in New York City, ACS Environ. Sci. Technol. Air, 1, 113–128, https://doi.org/10.1021/acsestair.3c00037, 2024.

Hou, S., Tong, S., Ge, M., and An, J.: Comparison of atmospheric nitrous acid during severe haze and clean periods in Beijing, China, Atmos. Environ., 124, 199–206, https://doi.org/10.1016/j.atmosenv.2015.06.023, 2016.

Huang, R.., Yang, L., Cao, J., Wang, Q., Tie, X., Ho, K., Shen, Z., Zhang, R., Li, G., Zhu, C., Zhang, N., Dai, W., Zhou, J., Liu, S., Chen, Y., Chen, J., and O'Dowd, C. D.: Concentration and sources of atmospheric nitrous acid (HONO) at an urban site in Western China, Sci. Total Environ., 593–594, 165–172, https://doi.org/10.1016/j.scitotenv.2017.02.166, 2017.

Kim, M. and Or, D.: Microscale pH variations during drying of soils and desert biocrusts affect HONO and NH_3 emissions, Nat. Commun., 10, 3944, https://doi.org/10.1038/s41467-019-11956-6, 2019.

Kong, L., Tang, X., Zhu, J., Wang, Z., Liu, B., Zhu, Y., Zhu, L., Chen, D., Hu, K., Wu, H., Wu, Q., Shen, J., Sun, Y., Liu, Z., Xin, J., Ji, D., and Zheng, M.: High-resolution simulation dataset of hourly $PM_{2.5}$ chemical composition in China (CAQRA-aerosol) from 2013 to 2020, Adv. Atmos. Sci., 41, 1–16, 2024.

Kurtenbach, R., Becker, K. H., Gomes, J. A. G., Kleffmann, J., Lörzer, J. C., Spittler, M., Wiesen, P., Ackermann, R., Geyer, A., and Platt, U.: Investigations of emissions and heterogeneous formation of HONO in a road traffic tunnel, Atmos. Environ., 35, 3385–3394, https://doi.org/10.1016/S1352-2310(01)00138-8, 2001.

Lee, J. D., Whalley, L. K., Heard, D. E., Stone, D., Dunmore, R. E., Hamilton, J. F., Young, D. E., Allan, J. D., Laufs, S., and Kleffmann, J.: Detailed budget analysis of HONO in central London reveals a missing daytime source, Atmos. Chem. Phys., 16, 2747–2764, https://doi.org/10.5194/acp-16-2747-2016, 2016.

Li, D., Xue, L., Wen, L., Wang, X., Chen, T., Mellouki, A., Chen, J., and Wang, W.: Characteristics and sources of nitrous acid in an urban atmosphere of northern China: Results from 1-yr continuous observations, Atmos. Environ., 182, 296–306, https://doi.org/10.1016/j.atmosenv.2018.03.033, 2018.

Li, W., Tong, S., Cao, J., Su, H., Zhang, W., Wang, L., Jia, C., Zhang, X., Wang, Z., Chen, M., and Ge, M.: Comparative observation of atmospheric nitrous acid (HONO) in Xi'an and Xianyang located in the GuanZhong basin of western China, Environ. Pollut., 289, 117679, https://doi.org/10.1016/j.envpol.2021.117679, 2021.

Li, X., Brauers, T., Häseler, R., Bohn, B., Fuchs, H., Hofzumahaus, A., Holland, F., Lou, S., Lu, K. D., Rohrer, F., Hu, M., Zeng, L. M., Zhang, Y. H., Garland, R. M., Su, H., Nowak, A., Wiedensohler, A., Takegawa, N., Shao, M., and Wahner, A.: Exploring the atmospheric chemistry of nitrous acid (HONO) at a rural site in Southern China, Atmos. Chem. Phys., 12, 1497–1513, https://doi.org/10.5194/acp-12-1497-2012, 2012.

Li, Y., An, J., Min, M., Zhang, W., Wang, F., and Xie, P.: Impacts of HONO sources on the air quality in Beijing, Tianjin and Hebei Province of China, Atmos. Environ., 45, 4735–4744, https://doi.org/10.1016/j.atmosenv.2011.04.086, 2011.

Li, Z., Ren, Z., Liu, C., Ning, Z., Liu, J., Liu, J., Zhai, Z., Ma, X., Chen, L., Zhang, Y., Bai, L., and Kong, S.: Heterogeneous variations in wintertime $PM_{2.5}$ sources, compositions and exposure risks at urban/suburban rural/remote rural areas in the post COVID-19/Clean-Heating period, Atmos. Environ., 326, 120463, https://doi.org/10.1016/j.atmosenv.2024.120463, 2024.

Lian, C., Wang, W., Chen, Y., Zhang, Y., Zhang, J., Liu, Y., Fan, X., Li, C., Zhan, J., Lin, Z., Hua, C., Zhang, W., Liu, M., Li, J., Wang, X., An, J., and Ge, M.: Long-term winter observation of nitrous acid in the urban area of Beijing, J. Environ. Sci. (China), 114, 334–342, https://doi.org/10.1016/j.jes.2021.09.010, 2022.

Liang, Y., Zha, Q., Wang, W., Cui, L., Lui, K. H., Ho, K. F., Wang, Z., Lee, S., and Wang, T.: Revisiting nitrous acid (HONO) emission from on-road vehicles: A tunnel study with a mixed fleet, J. Air Waste Manage., 67, 797–805, https://doi.org/10.1080/10962247.2017.1293573, 2017.

Liao, S., Zhang, J., Yu, F., Zhu, M., Liu, J., Ou, J., Dong, H., Sha, Q., Zhong, Z., Xie, Y., Luo, H., Zhang, L., and Zheng, J.: High gaseous nitrous acid (HONO) emissions from light-duty diesel vehicles, Environ. Sci. Technol., 55, 200–208, https://doi.org/10.1021/acs.est.0c05599, 2021.

Liu, P., Zhang, C., Mu, Y., Liu, C., Xue, C., Ye, C., Liu, J., Zhang, Y., and Zhang, H.: The possible contribution of the periodic emissions from farmers' activities in the North China Plain to atmospheric water-soluble ions in Beijing, Atmos. Chem. Phys., 16, 10097–10109, https://doi.org/10.5194/acp-16-10097-2016, 2016.

Liu, P., Zhang, C., Xue, C., Mu, Y., Liu, J., Zhang, Y., Tian, D., Ye, C., Zhang, H., and Guan, J.: The contribution of residential coal combustion to atmospheric $PM_{2.5}$ in northern China during winter, Atmos. Chem. Phys., 17, 11503–11520, https://doi.org/10.5194/acp-17-11503-2017, 2017.

Liu, Y., Lu, K., Li, X., Dong, H., Tan, Z., Wang, H., Zou, Q., Wu, Y., Zeng, L., Hu, M., Min, K.-E., Kecorius, S., Wiedensohler, A., and Zhang, Y.: A comprehensive model test of the HONO sources constrained to field measurements at rural North China Plain, Environ. Sci. Technol., 53, 3517–3525, https://doi.org/10.1021/acs.est.8b06367, 2019.

Monge, M. E., D'Anna, B., Mazri, L., Giroir-Fendler, A., Ammann, M., Donaldson, D. J., and George, C.: Light changes the atmospheric reactivity of soot, P. Natl. Acad. Sci. USA, 107, 6605–6609, https://doi.org/10.1073/pnas.0908341107, 2010.

Mora Garcia, S. L., Pandit, S., Navea, J. G., and Grassian, V. H.: Nitrous acid (HONO) formation from the irradiation of aqueous nitrate solutions in the presence of marine chromophoric dissolved organic matter: comparison to other organic photosensitizers, ACS Earth Space Chem., 5, 3056–3064, https://doi.org/10.1021/acsearthspacechem.1c00292, 2021.

Oswald, R., Behrendt, T., Ermel, M., Wu, D., Su, H., Cheng, Y., Breuninger, C., Moravek, A., Mougin, E., Delon, C., Loubet, B., Pommerening-Roser, A., Sorgel, M., Poschl, U., Hoffmann, T., Andreae, M. O., Meixner, F. X., and Trebs, I.: HONO emissions from soil bacteria as a major source of atmospheric reactive nitrogen, Science, 341, 1233–1235, https://doi.org/10.1126/science.1242266, 2013.

Pipalatkar, P., Khaparde, V. V., Gajghate, D. G., and Bawase, M. A.: Source apportionment of $PM_{2.5}$ using a CMB model for a centrally located Indian city, Aerosol Air Qual. Res., 14, 1089–1099, https://doi.org/10.4209/aaqr.2013.04.0130, 2014.

Reeser, D. I., Kwamena, N.-O. A., and Donaldson, D. J.: Effect of organic coatings on gas-phase nitrogen dioxide production from aqueous nitrate photolysis, J. Phys. Chem. C, 117, 22260–22267, https://doi.org/10.1021/jp401545k, 2013.

Ren, X., Harder, H., Martinez, M., Lesher, R. L., Oliger, A., Simpas, J. B., Brune, W. H., Schwab, J. J., Demerjian, K. L., He, Y., Zhou, X., and Gao, H.: OH and HO_2 Chemistry in the urban atmosphere of New York City, Atmos. Environ., 37, 3639–3651, https://doi.org/10.1016/S1352-2310(03)00459-X, 2003.

Romer, P. S., Wooldridge, P. J., Crounse, J. D., Kim, M. J., Wennberg, P. O., Dibb, J. E., Scheuer, E., Blake, D. R., Meinardi, S., Brosius, A. L., Thames, A. B., Miller, D. O., Brune, W. H., Hall, S. R., Ryerson, T. B., and Cohen, R. C.: Constraints on aerosol nitrate photolysis as a potential source of HONO and NO_x, Environ. Sci. Technol., 52, 13738–13746, https://doi.org/10.1021/acs.est.8b03861, 2018.

Scharko, N. K., Berke, A. E., and Raff, J. D.: Release of nitrous acid and nitrogen dioxide from nitrate photolysis in acidic aqueous solutions, Environ. Sci. Technol., 48, 11991–12001, https://doi.org/10.1021/es503088x, 2014.

Shi, Q., Tao, Y., Krechmer, J. E., Heald, C. L., Murphy, J. G., Kroll, J. H., and Ye, Q.: Laboratory investigation of renoxification from the photolysis of inorganic particulate nitrate, Environ. Sci. Technol., 55, 854–861, https://doi.org/10.1021/acs.est.0c06049, 2021.

Slater, E. J., Whalley, L. K., Woodward-Massey, R., Ye, C., Lee, J. D., Squires, F., Hopkins, J. R., Dunmore, R. E., Shaw, M., Hamilton, J. F., Lewis, A. C., Crilley, L. R., Kramer, L., Bloss, W., Vu, T., Sun, Y., Xu, W., Yue, S., Ren, L., Acton, W. J. F., Hewitt, C. N., Wang, X., Fu, P., and Heard, D. E.: Elevated levels of OH observed in haze events during wintertime in central Beijing, Atmos. Chem. Phys., 20, 14847–14871, https://doi.org/10.5194/acp-20-14847-2020, 2020.

Stemmler, K., Ammann, M., Donders, C., Kleffmann, J., and George, C.: Photosensitized reduction of nitrogen dioxide on humic acid as a source of nitrous acid, Nature, 440, 195–198, https://doi.org/10.1038/nature04603, 2006.

Su, H., Cheng, Y. F., Shao, M., Gao, D. F., Yu, Z. Y., Zeng, L. M., Slanina, J., Zhang, Y. H., and Wiedensohler, A.: Nitrous acid (HONO) and its daytime sources at a rural site during the 2004 PRIDE-PRD experiment in China, J. Geophys. Res.-Atmos., 113, D14312, https://doi.org/10.1029/2007jd009060, 2008.

Su, H., Cheng, Y., Oswald, R., Behrendt, T., Trebs, I., Meixner, F. X., Andreae, M. O., Cheng, P., Zhang, Y., and Poschl, U.: Soil nitrite as a source of atmospheric HONO and OH radicals, Science, 333, 1616–1618, https://doi.org/10.1126/science.1207687, 2011.

Svoboda, O., Kubelová, L., and Slavíček, P.: Enabling forbidden processes: quantum and solvation enhancement of nitrate anion UV absorption, J. Phys. Chem. A, 117, 12868–12877, https://doi.org/10.1021/jp4098777, 2013.

Villena, G., Wiesen, P., Cantrell, C. A., Flocke, F., Fried, A., Hall, S. R., Hornbrook, R. S., Knapp, D., Kosciuch, E., Mauldin, R. L., McGrath, J. A., Montzka, D., Richter, D., Ullmann, K., Walega, J., Weibring, P., Weinheimer, A., Staebler, R. M., Liao, J., Huey, L. G., and Kleffmann, J.: Nitrous acid (HONO) during polar spring in Barrow, Alaska: A net source of OH radicals?, J. Geophys. Res., 116, D00R07, https://doi.org/10.1029/2011jd016643, 2011.

Wang, H., Ding, J., Xu, J., Wen, J., Han, J., Wang, K., Shi, G., Feng, Y., Ivey, C. E., Wang, Y., Nenes, A., Zhao, Q., and Russell, A. G.: Aerosols in an arid environment: The role of aerosol water content, particulate acidity, precursors, and relative humidity on secondary inorganic aerosols, Sci. Total Environ., 646, 564–572, https://doi.org/10.1016/j.scitotenv.2018.07.321, 2019.

Wang, J., Zhang, X., Guo, J., Wang, Z., and Zhang, M.: Observation of nitrous acid (HONO) in Beijing, China: Seasonal variation, nocturnal formation and daytime budget, Sci. Total Environ., 587–588, 350–359, https://doi.org/10.1016/j.scitotenv.2017.02.159, 2017.

Wang, J., Gao, J., Che, F., Wang, Y., Lin, P., and Zhang, Y.: Decade-long trends in chemical component properties of $PM_{2.5}$ in Beijing, China (2011–2020), Sci. Total Environ., 832, 154664, https://doi.org/10.1016/j.scitotenv.2022.154664, 2022a.

Wang, J., Gao, J., Che, F., Wang, Y., Lin, P., and Zhang, Y.: Dramatic changes in aerosol composition during the 2016–2020 heating seasons in Beijing–Tianjin–Hebei region and its surrounding areas: The role of primary pollutants and secondary aerosol formation, Sci. Total. Environ., 849, 157621, https://doi.org/10.1016/j.scitotenv.2022.157621, 2022b.

Wang, Y., Huang, D. D., Huang, W., Liu, B., Chen, Q., Huang, R., Gen, M., Mabato, B. R. G., Chan, C. K., Li, X., Hao, T., Tan, Y., Hoi, K. I., Mok, K. M., and Li, Y. J.: Enhanced nitrite production from the aqueous photolysis of nitrate in the presence of vanillic acid and implications for the roles of light-absorbing organics, Environ. Sci. Technol., 55, 15694–15704, https://doi.org/10.1021/acs.est.1c04642, 2021.

Wang, Y., Xiao, S., Zhang, Y., Chang, H., Martin, R. V., Van Donkelaar, A., Gaskins, A., Liu, Y., Liu, P., and Shi, L.: Long-term exposure to $PM_{2.5}$ major components and mortality in the southeastern United States, Environ. Int., 158, 106969, https://doi.org/10.1016/j.envint.2021.106969, 2022.

Wang, Y., Fu, X., Wang, T., Ma, J., Gao, H., Wang, X., and Pu, W.: Large contribution of nitrous acid to soil-emitted reactive oxidized nitrogen and its effect on air quality, Environ. Sci. Technol., 57, 3516–3526, https://doi.org/10.1021/acs.est.2c07793, 2023.

Wang, Z., Zhang, D., Liu, B., Li, Y., Chen, T., Sun, F., Yang, D., Liang, Y., Chang, M., Yang, L., and Lin, A.: Analysis of chemical characteristics of $PM_{2.5}$ in Beijing over a 1-year period, J. Atmos. Chem., 73, 407–425, https://doi.org/10.1007/s10874-016-9334-8, 2016.

Wexler, A. S. and Clegg, S. L.: Atmospheric aerosol models for systems including the ions H^+, NH_4^+, Na^+, SO_4^{2-}, NO_3^-, Cl^-, Br^-, and H_2O, J. Geophys. Res.-Atmos., 107, ACH 14-1–ACH 14-14, https://doi.org/10.1029/2001JD000451, 2002.

Xiao, H.-W., Xiao, H.-Y., Luo, L., Shen, C.-Y., Long, A.-M., Chen, L., Long, Z.-H., and Li, D.-N.: Atmospheric aerosol compositions over the South China Sea: temporal variability and source apportionment, Atmos. Chem. Phys., 17, 3199–3214, https://doi.org/10.5194/acp-17-3199-2017, 2017.

Yang, W., Han, C., Yang, H., and Xue, X.: Significant HONO formation by the photolysis of nitrates in the presence of humic acids, Environ. Pollut., 243, 679–686, https://doi.org/10.1016/j.envpol.2018.09.039, 2018.

Ye, C., Gao, H., Zhang, N., and Zhou, X.: Photolysis of nitric acid and nitrate on natural and artificial surfaces, Environ. Sci. Technol., 50, 3530–3536, https://doi.org/10.1021/acs.est.5b05032, 2016a.

Ye, C., Zhou, X., Pu, D., Stutz, J., Festa, J., Spolaor, M., Tsai, C., Cantrell, C., Mauldin, R. L., Campos, T., Weinheimer, A., Hornbrook, R. S., Apel, E. C., Guenther, A., Kaser, L., Yuan, B., Karl, T., Haggerty, J., Hall, S., Ullmann, K., Smith, J. N., Ortega, J., and Knote, C.: Rapid cycling of reactive nitrogen in the marine boundary layer, Nature, 532, 489–491, https://doi.org/10.1038/nature17195, 2016b.

Ye, C., Zhang, N., Gao, H., and Zhou, X.: Photolysis of particulate nitrate as a source of HONO and NO_x, Environ. Sci. Technol., 51, 6849–6856, https://doi.org/10.1021/acs.est.7b00387, 2017.

Ye, C., Zhang, N., Gao, H., and Zhou, X.: Matrix effect on surface-catalyzed photolysis of nitric acid, Sci. Rep., 9, 4351, https://doi.org/10.1038/s41598-018-37973-x, 2019.

Zhang, L., Wang, T., Zhang, Q., Zheng, J., Xu, Z., and Lv, M.: Potential sources of nitrous acid (HONO) and their impacts on ozone: A WRF-Chem study in a polluted subtropical region, J. Geophys. Res.-Atmos., 121, 3645–3662, https://doi.org/10.1002/2015JD024468, 2016.

Zhang, R., Gen, M., Huang, D., Li, Y., and Chan, C. K.: Enhanced sulfate production by nitrate photolysis in the presence of halide ions in atmospheric particles, Environ. Sci. Technol., 54, 3831–3839, https://doi.org/10.1021/acs.est.9b06445, 2020.

Zhang, W., Tong, S., Jia, C., Wang, L., Liu, B., Tang, G., Ji, D., Hu, B., Liu, Z., Li, W., Wang, Z., Liu, Y., Wang, Y., and Ge, M.: Different HONO sources for three layers at the urban area of Beijing, Environ. Sci. Technol., 54, 12870–12880, https://doi.org/10.1021/acs.est.0c02146, 2020.

Zheng, J., Shao, M., Che, W., Zhang, L., Zhong, L., Zhang, Y., and Streets, D.: Speciated VOC emission inventory and spatial patterns of ozone formation potential in the Pearl River Delta, China, Environ. Sci. Technol., 43, 8580–8586, https://doi.org/10.1021/es901688e, 2009.

Zhou, X., Gao, H., He, Y., Huang, G., Bertman, S. B., Civerolo, K., and Schwab, J.: Nitric acid photolysis on surfaces in low-NO_x environments: Significant atmospheric implications, Geophys. Res. Let., 30, 2217, https://doi.org/10.1029/2003GL018620, 2003.

Zhou, X., Zhang, N., TerAvest, M., Tang, D., Hou, J., Bertman, S., Alaghmand, M., Shepson, P. B., Carroll, M. A., Griffith, S., Dusanter, S., and Stevens, P. S.: Nitric acid photolysis on forest canopy surface as a source for tropospheric nitrous acid, Nat. Geosci., 4, 440–443, https://doi.org/10.1038/ngeo1164, 2011.